

Chiral orbital order of interacting bosons without higher bands

Marco Di Liberto^{1,2,3,*} and Nathan Goldman^{4,†}

¹*Dipartimento di Fisica e Astronomia “G. Galilei” & Padua Quantum Technologies Research Center, Università degli Studi di Padova, I-35131, Padova, Italy*

²*INFN Istituto Nazionale di Fisica Nucleare, Sezione di Padova, I-35131, Padova, Italy*

³*Institute for Quantum Optics and Quantum Information of the Austrian Academy of Sciences, Innsbruck, Austria*

⁴*Center for Nonlinear Phenomena and Complex Systems, Université Libre de Bruxelles, CP 231, Campus Plaine, B-1050 Brussels, Belgium*

Ultracold atoms loaded into higher Bloch bands provide an elegant setting for realizing many-body quantum states that spontaneously break time-reversal symmetry through the formation of chiral orbital order. The applicability of this strategy remains nonetheless limited due to the finite lifetime of atoms in high-energy bands. Here we introduce an alternative framework, suitable for bosonic gases, which builds on assembling square plaquettes pierced by a π -flux (half a magnetic-flux quantum). This setting is shown to be formally equivalent to an interacting bosonic gas loaded into p orbitals, and we explore the consequences of the resulting chiral orbital order, both for weak and strong onsite interactions. We demonstrate the emergence of a chiral superfluid vortex lattice, exhibiting a long-lived gapped collective mode that is characterized by local chiral currents. This chiral superfluid phase is shown to undergo a phase transition to a chiral Mott insulator for sufficiently strong interactions. Our work establishes coupled π -flux plaquettes as a practical route for the emergence of orbital order and chiral phases of matter.

Introduction. Breaking time-reversal symmetry is known to drastically alter the phases and dynamical properties of quantum matter, as was evidenced by vortex lattices in rotating ultracold gases [1–3] and the quantum Hall effects in 2D materials immersed in strong magnetic fields [4]. In the context of cold atoms in optical lattices, this fundamental symmetry can be broken by privileging a certain orientation of motion, e.g. by rotating the system [3, 5] or by applying a circular shaking to the lattice [6, 7]. However, these methods lead to instabilities or heating, hence complicating the formation of strongly-correlated phases [3, 8]. This motivates the development of alternative schemes to break time-reversal symmetry in ultracold gases.

A first possible route builds on addressing different internal states of an atom with lasers, in view of engineering synthetic lattice structures with effective magnetic fluxes [9–15]. Such schemes have been experimentally implemented and lead to the observation of chiral states and dynamics [16–20]. A second route exploits the orbital structure of higher Bloch bands [21, 22] in the absence of external driving. In these systems, interactions couple the different orbitals and can favour ground states with finite angular momentum, thus spontaneously breaking time-reversal symmetry [23]. The realization of higher-band lattice models offers the opportunity to observe intriguing correlated quantum phases with chiral properties [24–31] as well as topological chiral excitations [32, 33]. Quantum gases have been experimentally loaded into p bands [34, 35], as well as higher bands [36], hence leading to the observation of short-lived condensates with spontaneously broken time-reversal symmetry [35, 37, 38]. However, atoms in higher bands have a relatively short lifetime due to atom-atom collisions, thus making

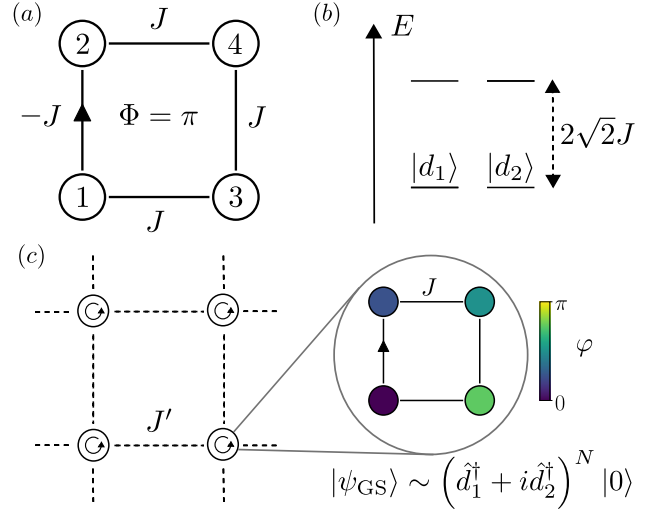


Figure 1. The π -flux plaquette building block for chiral bosonic phases. (a) Schematic representation of a single plaquette with flux $\Phi = \pi$. (b) Single-particle spectrum displaying two-fold degeneracy separated by an energy gap. (c) Sketch of an extended lattice of connected building-blocks, with $J' \ll J$, resulting in a chiral superfluid phase: each super-site hosts a quantized vortex associated with the condensate phase winding, $\varphi_i = \arg(\hat{b}_i)$.

it challenging to reach the strongly-interacting regime.

In this work, we introduce an alternative route to p -band orbital physics, which does not rely on populating higher bands. Our approach is based on an analogy between $p_{x,y}$ orbitals and the two-fold degenerate low-energy orbitals $d_{1,2}$ provided by a square plaquette pierced by a π -flux [Figs. 1(a)-(b)]. Considering bosons with Hubbard interactions, we show that this setting favors chiral orbital order and breaks time-reversal sym-

metry. Our construction consists in coupling these π -flux plaquettes with weak links, such as to preserve the orbital order over extended lattices [Fig. 1(c)]. We explore this approach both in the weakly and strongly-interacting regimes. In particular, we demonstrate the emergence of a chiral superfluid vortex phase, exhibiting a long-lived gapped collective mode and local chiral currents. Furthermore, we show that the superfluid undergoes a transition to a chiral Mott insulator for sufficiently strong interactions and half filling. Our results establish coupled π -flux plaquettes as powerful building blocks for orbital-like physics and chiral phases of matter.

Single-plaquette with π -flux: Effective theory. The interplay of magnetic flux and interactions can have remarkable effects, even at the level of a single plaquette [15, 39, 40]. Here, we start by considering a single square plaquette pierced by a π flux [see sketch in Fig. 1(a)], as described by

$$\hat{H}_0 = -J \left(e^{i\pi} \hat{b}_1^\dagger \hat{b}_2 + \hat{b}_2^\dagger \hat{b}_4 + \hat{b}_4^\dagger \hat{b}_3 + \hat{b}_3^\dagger \hat{b}_1 + \text{H.c.} \right), \quad (1)$$

with onsite Hubbard interactions among the bosons

$$\hat{H}_{\text{int}} = \frac{U}{2} \sum_i \hat{n}_i (\hat{n}_i - 1), \quad (2)$$

and we set $U > 0$ (repulsive). The full Hamiltonian reads $\hat{H} = \hat{H}_0 + \hat{H}_{\text{int}}$. The Hamiltonian \hat{H}_0 admits four eigenstates that are pairwise degenerate in energy, $\epsilon_{1,2} = -\sqrt{2}J$ and $\epsilon_{3,4} = \sqrt{2}J$; see Fig. 1(b). We indicate the operators corresponding to the modes with eigenvalues ϵ_i as \hat{d}_i , \hat{d}_i^\dagger , defined through the unitary transformation $\hat{b}_i = \sum_{ij} \mathcal{U}_{ij} \hat{d}_j$ [41, 42]. Since the single-particle theory displays an energy gap $\Delta\epsilon = 2\sqrt{2}J$, it is meaningful to consider the projected Hamiltonian $\hat{H}_{\text{eff}} \equiv \hat{P}\hat{H}\hat{P}$, where \hat{P} is the projection operator onto the low-energy subspace spanned by the modes with $i = 1, 2$ [43, 44]:

$$\hat{H}_{\text{eff}} = \frac{3U}{16} \hat{n}^2 - \frac{U}{16} \hat{L}_z^2 - \left(\sqrt{2}J + \frac{U}{8} \right) \hat{n}, \quad (3)$$

where $\hat{n} = \hat{d}_1^\dagger \hat{d}_1 + \hat{d}_2^\dagger \hat{d}_2$ and $\hat{L}_z = i(\hat{d}_1^\dagger \hat{d}_2 - \hat{d}_2^\dagger \hat{d}_1)$. This expression shows that the low-energy physics of weakly-interacting bosons in a π -flux plaquette shares similarities with p -band bosons [22]: In direct analogy with $p_{x,y}$ orbitals, the two modes d_1 and d_2 experience density-density repulsive interactions but also an orbital-like coupling $-\hat{L}_z^2$ with a *negative* sign. The operator \hat{L}_z has the same structure as the angular momentum operator built from $p_{x,y}$ orbitals, and the negative sign privileges a ground state with the highest angular momentum possible (for $U > 0$), i.e. a macroscopic occupation of a complex orbital $|d_1\rangle \pm i|d_2\rangle$ [22]. Besides the global $U(1)$ symmetry associated with the conservation of the total number of particles and time-reversal symmetry, the low-energy Hamiltonian displays an emergent discrete \mathbb{Z}_2

symmetry represented by $\hat{d}_1 \rightarrow \hat{d}_2$ and $\hat{d}_2 \rightarrow \hat{d}_1$, which transforms the angular momentum as $\hat{L}_z \rightarrow -\hat{L}_z$.

The Hamiltonian in Eq. (3) can be solved exactly by noting that $[\hat{L}_z, \hat{H}_{\text{eff}}] = 0$. Indicating the single-particle eigenstates of \hat{L}_z as $|\pm\rangle \equiv \hat{d}_\pm^\dagger |0\rangle$, with $\hat{L}_z |\pm\rangle = \pm |\pm\rangle$ and $\hat{d}_\pm^\dagger = (\hat{d}_1^\dagger \pm i\hat{d}_2^\dagger)/\sqrt{2}$, a generic many-body eigenstate with energy E_{eff} can therefore be written as

$$|n_+, n_-\rangle = \frac{1}{\sqrt{n_+! n_-!}} (\hat{d}_+^\dagger)^{n_+} (\hat{d}_-^\dagger)^{n_-} |0\rangle, \quad (4)$$

$$E_{\text{eff}}(n_+, n_-) = \frac{3UN^2}{16} - \frac{U}{16} (n_+ - n_-)^2 - \left(\sqrt{2}J + \frac{U}{8} \right) N,$$

with $N = n_+ + n_-$. The two-fold degenerate ground state thus corresponds to $n_+ = N$ or $n_- = N$, i.e. $|\psi_{\text{GS}}\rangle \sim \left(\hat{d}_1^\dagger \pm i\hat{d}_2^\dagger \right)^N |0\rangle$, with energy per particle $E_{\text{GS}}/N = g/8 - \sqrt{2}J - g/8N$. Such a ground state, which breaks the aforementioned time-reversal and \mathbb{Z}_2 symmetries [45], is a chiral condensate with angular momentum $\langle \hat{L}_z \rangle = \pm N$. Let us consider the ground state with positive chirality, $n_+ = N$. The lowest one-particle excitation, which is given by $n_+ = N - 1$ and $n_- = 1$, corresponds to removing a particle from the condensate and transferring it to a state with opposite angular momentum. The energy corresponding to this elementary excitation is $\Delta E_{\text{exc}} = g/4 - U/4$.

The collective mode on a single plaquette. To gain more insight on this excitation, we now discuss the weakly-interacting regime within a hydrodynamic approach relevant to systems of ultracold atoms and nonlinear photonics. We therefore consider a finite $g \equiv UN \ll J$, and take the limit $N \rightarrow \infty$. Under these assumptions, the problem is treated using a discrete Gross-Pitaevskii description with N condensed particles: we replace the operators in Eq. (3) by the ansatz

$$\hat{d}_1 \rightarrow \langle \hat{d}_1 \rangle = \sqrt{N_1}, \quad \hat{d}_2 \rightarrow \langle \hat{d}_2 \rangle = e^{i\theta} \sqrt{N_2}, \quad (5)$$

with $N = N_1 + N_2$, and construct the energy functional

$$E_{\text{MF}}[d_1, d_2] = E(N) - \frac{U}{4} N_1 (N - N_1) \sin^2 \theta, \quad (6)$$

where $E(N) = 3UN^2/16 - (\sqrt{2}J + U/8)N$. Note that the last term in Eq. (6), which corresponds to $-\hat{L}_z^2$, is minimized for $N_{1,2} = N/2$ and $\theta = \pm\pi/2$, thus breaking time-reversal symmetry. This yields the ground state energy per particle $E_{\text{GS}}^{\text{MF}}/N = -\sqrt{2}J + g/8$, which is in agreement with E_{GS}/N for $N \rightarrow \infty$.

The eigenmodes of the condensate can be obtained by studying the fluctuations with respect to the stationary solution. We introduce the Lagrangian density

$$\mathcal{L} = i(d_1^* \partial_t d_1 + d_2^* \partial_t d_2) - E_{\text{MF}}[d_1, d_2], \quad (7)$$

and define small fluctuations within a hydrodynamic picture as $N_{1,2} \rightarrow N/2 \pm \delta\rho$ and $\theta \rightarrow \pi/2 + \delta\theta$. At lowest

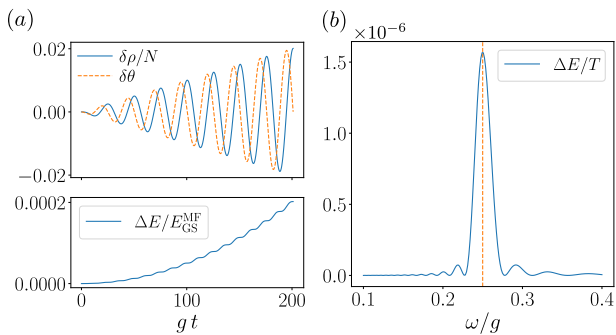


Figure 2. Exciting the collective mode by driving. (a) Phase and density dynamics at resonance $\omega = \omega_0 = g/4$ and corresponding energy absorption for $V_0 = 10^{-4}g$. (b) Resonance peak obtained by measuring the absorption energy rate over $t = 10T$, where $T = 2\pi/\omega$. The vertical dashed line is drawn at the expected resonance condition $\omega = g/4$.

order, we obtain $E_{\text{MF}}[d_1, d_2] = E_{\text{MF}}^{(0)} + \delta E_{\text{MF}}^{(2)}$, where

$$\delta E_{\text{MF}}^{(2)} = \frac{UN^2}{16}\delta\theta^2 + \frac{U}{4}\delta\rho^2. \quad (8)$$

The dynamical variables are the relative density and the relative phase, satisfying the equations of motion $\partial_t\delta\theta = \frac{U}{2}\delta\rho$ and $\partial_t\delta\rho = -\frac{UN^2}{8}\delta\theta$, which have the solutions

$$\delta\theta = A \cos \omega_0 t, \quad \delta\rho = -\frac{AN}{2} \sin \omega_0 t, \quad (9)$$

with $\omega_0 = g/4$ and A an arbitrary constant set by the initial conditions. As a distinctive signature of the mode, the oscillation of the two conjugate variables occurs with a phase difference $\pi/2$. The nature of this mode shares similarities with a recent measurement in p bands [46, 47].

Detecting the collective mode. We now show how to detect the collective mode via spectroscopy or quench protocols. We first consider a time-periodic modulation of the onsite energy at two opposite corners of the plaquette,

$$\begin{aligned} \delta\hat{V} &= V(t)(\hat{b}_2^\dagger\hat{b}_2 - \hat{b}_3^\dagger\hat{b}_3) \\ &\approx \frac{V(t)}{2}(\hat{d}_2^\dagger\hat{d}_2 - \hat{d}_1^\dagger\hat{d}_1) \rightarrow -V(t)\delta\rho, \end{aligned} \quad (10)$$

with $V(t) = V_0 \sin \omega t$. As shown by Eq. (10), this spectroscopic probe couples to the relative density $\delta\rho$ within the projected theory. When reaching resonance, $\omega = \omega_0 = g/4$, the system is expected to absorb energy while populating the collective mode characterized by Eq. (9). This is confirmed in Fig. 2(a), which shows a numerical integration of the full nonlinear equations of motion, obtained from the Lagrangian (7) with the addition of the drive $\delta\hat{V}(t)$. One recognizes the characteristic $\pi/2$ phase difference between the relative density $\delta\rho$ and relative phase $\delta\theta$ [Eq. (9)]. In Fig. 2(b), the energy absorption per unit period of driving shows a peak at $\omega = \omega_0$, confirming our analysis.

The exact solution in Eq. (4) already revealed that the excited mode corresponds to a single-particle excitation carrying angular momentum. This translates into a real-space current that can be detected by the following quench protocol. Inspired by the dynamics of density defects in topological systems [48–50], we introduce a small onsite “impurity” potential $\Delta\hat{H} = -\Delta\hat{b}_1^\dagger\hat{b}_1$, with $\Delta > 0$ and $\Delta \ll g \ll J$. This creates an initial state with a small excess density on one site. The energy functional $E_{\text{MF}}(\theta)/\rho = (g/32)\cos 2\theta + (\Delta/4)\cos\theta$ shows that this state corresponds to occupying a small fraction of the excited mode (of the unperturbed system) with $\theta = \arccos(-2\Delta/g) \neq \pm\pi/2$. At $t=0$, we then quench $\Delta \rightarrow 0$ and let the system evolve in time. The real-space dynamics is obtained by directly solving the 4-sites Gross-Pitaevskii (GP) equations $i\partial_t b_i = -\sum_j J_{ij}b_j + U|b_i|^2 b_i$; it displays a clear chiral motion of the impurity, as shown in Fig. 3(a). These results were benchmarked by computing the dynamics of the full many-body system, using exact-diagonalization (ED) [51]. Figure 3(b) shows a scaling analysis of the extracted oscillation frequency in the $N \rightarrow \infty$ limit, confirming the GP results at short times. We attribute the small mismatch with the projected theory result ($\omega = g/4$) to the perturbative contribution of the high-energy orbitals.

Chiral phases in extended lattices. Having established the chiral properties emerging from bosonic π -flux plaquettes, we now demonstrate how assembling these building blocks can lead to chiral phases of matter, both in the weakly and strongly interacting regimes. Our construction consists in connecting π -flux plaquettes with weak couplings $J' \ll J$, such that each plaquette can be viewed as a super-site hosting two orbitals (in direct analogy with p -band models [52, 53]). Considering

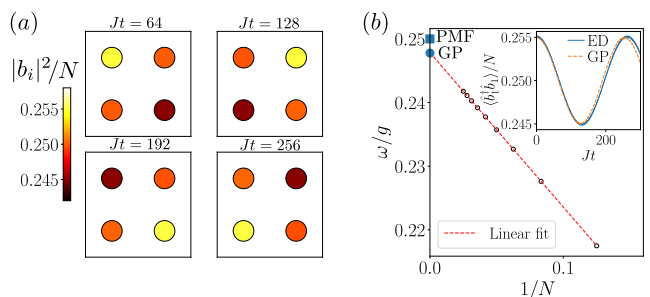


Figure 3. Chiral impurity dynamics. (a) Snapshots of the density distribution at different times showing the chiral motion of the impurity for $\Delta = 0.001J$ and $g = 0.1J$ obtained from the full GP dynamics. (b) Oscillation frequency for $g = 0.1J$ obtained by ED for different particle numbers N and scaling for $N \rightarrow \infty$. The solid square indicates the projected mean-field (PMF) theory result $g/4$ and the solid circle indicates the GP oscillation frequency. In the inset, single-site density dynamics obtained within the GP description compared with ED for $N = 32$ and $U = g/N$.

a square geometry [Fig. 4(a)], this naturally leads us to an interacting bosonic version of the BBH model [54], initially introduced in the context of higher-order topological insulators.

We define the projected orbital operators acting on each plaquette as $\hat{d}_{1,\mathbf{r}}$ and $\hat{d}_{2,\mathbf{r}}$, where \mathbf{r} indicates the plaquettes position. The local terms describing the dynamics within each plaquette are represented by the Hamiltonian (3). Upon projection (\hat{P}), the new inter-plaquette terms (J') are described by

$$\hat{H}'_{\text{eff}} = -\frac{J'}{2\sqrt{2}} \sum_{\mathbf{r},\sigma,\nu} \left(\hat{d}_{\sigma,\mathbf{r}}^\dagger \hat{d}_{\sigma,\mathbf{r}+\mathbf{e}_\nu} + \text{H.c.} \right), \quad (11)$$

where $\mathbf{e}_x = (a, 0)$, $\mathbf{e}_y = (0, a)$ and a is the lattice constant. In the weakly-interacting limit, the ground state is a uniform condensate (Γ point) forming a superfluid vortex lattice [55], with the condensate phase pattern shown in Fig. 4(a); this simply repeats the single plaquette result indicated in Fig. 1. To study the fate of the chiral mode identified in a single plaquette, we perform a Bogoliubov analysis. We obtain the Bogoliubov Hamil-

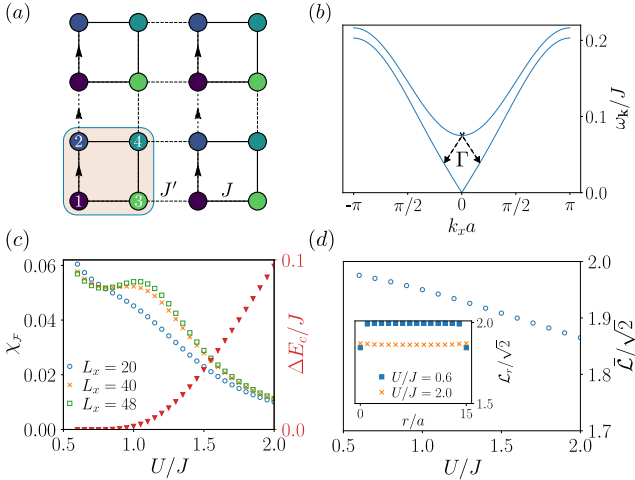


Figure 4. Interacting BBH model. (a) Tight-binding representation of the BBH model with uniform π -flux and staggered hopping amplitudes J , J' . The color of each site represents the ground state phase pattern for the weakly-interacting superfluid vortex lattice (units as in Fig. 1). (b) Bogoliubov spectrum within the projected theory for $J' = 0.1J$ and $g = 0.1J$, showing the appearance of a gapless and a gapped mode at small momenta. Dashed lines indicate the decay channel with rate Γ for the vortex excitation discussed in the main text. (c) Fidelity susceptibility $\chi_{\mathcal{F}}$ for a ladder with $L_y = 2$ sites and up to $L_x = 48$ sites, extracted with DMRG for $J' = 0.1J$. The peak indicates a phase transition, from a superfluid to an insulating phase, as further evidenced by the finite charge gap ΔE_c obtained by finite-size scaling. (d) Averaged loop-current $\hat{\mathcal{L}} \equiv \sum_r |\langle \hat{\mathcal{L}}_r \rangle| / N_p$ over the ladder plaquettes for $L_x = 32$, showing that time-reversal symmetry remains broken across the transition. The inset shows two profiles of loop-current patterns across the transition.

tonian $\hat{H}^{\text{Bog}} = \sum_{\mathbf{k} \neq 0, \alpha} \omega_{\alpha,\mathbf{k}} \hat{\beta}_{\alpha,\mathbf{k}}^\dagger \hat{\beta}_{\alpha,\mathbf{k}}$, with $\alpha = 1, 2$. Here $\hat{\beta}_{\alpha,\mathbf{k}}^\dagger$ creates a Bogoliubov quasiparticle and the spectrum reads $\omega_{1,\mathbf{k}} = \sqrt{\xi_{\mathbf{k}}(\xi_{\mathbf{k}} + g)}$ and $\omega_{2,\mathbf{k}} = g/4 + \xi_{\mathbf{k}}$, with $\xi_{\mathbf{k}} \equiv -J'(\cos k_x a + \cos k_y a - 2)/\sqrt{2}$. The two branches of the spectrum are shown in Fig. 4(b). The massless (Goldstone) mode at small momenta becomes $\omega_{1,\mathbf{k}} \approx c_s |\mathbf{k}|$ with the sound velocity $c_s = \sqrt{J'g/4\sqrt{2}}$, while the massive mode has a gap $g/4$, which corresponds to the single-plaquette gapped mode of energy ω_0 .

In the limit of disconnected plaquettes, $J' \ll g$, the excited mode is long lived as there is no lower energy mode to decay to. As the coupling strength approaches $J' \sim g$, the massive mode becomes energetically resonant with the gapless phonon branch, thus opening a direct channel for its decay. Within the effective projected theory, we computed the couplings $\hat{H}^{(3)}$ between the massive and massless modes up to cubic powers of $\delta \hat{d}_{\alpha,\mathbf{k}}^{(\dagger)}$. Assuming $g \ll J'$, the decay rate of the massive mode can be estimated as $\Gamma = \pi \sum_{\mathbf{q}} \delta(\omega_0 - 2\epsilon_{1,\mathbf{q}}) |\langle \beta_{1,\mathbf{q}} \beta_{1,-\mathbf{q}} | \hat{H}^{(3)} | \beta_{2,0} \rangle|^2 = 0.73\pi^2 g U / (512J')$ [42], thus suggesting that the mode is well defined ($\Gamma \lesssim \omega_0 = g/4$) under the condition $U \lesssim 17.85J'$.

From the effective (projected) model, and for appropriate filling factors, we expect a phase transition from the chiral superfluid to a chiral Mott insulator, governed by a competition between U and J' . However, whether this transition does take place in the bosonic BBH model is not obvious, as strong interactions can potentially lead to a breakdown of the effective theory. We now rigorously demonstrate the existence of this exotic phase transition by performing density-matrix renormalization group (DMRG) calculations [56] on a ladder version of the bosonic BBH model. In Fig. 4(c), we consider a ladder with $L_y = 2$ sites and up to $L_x = 48$ sites ($N_p = L_x/2$ plaquettes) with filling $\nu = 1/2$, namely two bosons per plaquette. The transition is identified by computing the fidelity susceptibility $\chi_{\mathcal{F}} = -(2/L_x) \lim_{\delta U \rightarrow 0} \partial^2 \mathcal{F} / \partial \delta U^2$ [57–59], where $\mathcal{F}(\delta U) = |\langle \Psi(U) | \Psi(U + \delta U) \rangle|$. Our results show the appearance of a clear peak in $\chi_{\mathcal{F}}$, located around $U \sim J$ for $J' = 0.1J$, which grows with the system size. For comparison, we solved the effective p -band-type model described by Eqs. (3) and (11), and found that the expected transition [29] indeed occurs in the same range as for the full BBH model [Fig. 4(c)], thus indicating that the projected theory provides a valid description across the transition. In addition to the fidelity peak, we also observed the opening of a charge gap $\Delta E_c = E(N+1) + E(N-1) - 2E(N)$, indicating that the system enters an incompressible phase known as chiral Mott insulator [29, 46], which is characterized by a finite angular momentum in each plaquette. This is confirmed by our calculation of the loop current operator $\hat{\mathcal{L}}_r = i \left(\hat{b}_{1,r}^\dagger \hat{b}_{3,r} + \hat{b}_{3,r}^\dagger \hat{b}_{4,r} + \hat{b}_{4,r}^\dagger \hat{b}_{2,r} - \hat{b}_{2,r}^\dagger \hat{b}_{1,r} - \text{H.c.} \right) \approx \sqrt{2} \hat{\mathcal{L}}_{z,r}$, which remains approximately constant across

the transition [Fig. 4(d)]. In contrast with p -bands, where angular momentum displays an antiferromagnetic ordering [29], the chiral Mott insulator exhibited by the bosonic BBH model exhibits a ferromagnetic ordering.

Concluding remarks. Our construction offers the opportunity to observe chiral bosonic phases deep in the strongly-correlated regime, which have remained elusive in higher bands [29] or in driven systems realizing synthetic flux [60, 61]. Besides, an interesting perspective concerns the possible interplay between the interacting bosonic phases presented in this work and the unusual topological properties of the underlying BBH band structure [41, 54]; see also Refs. [62–65] on interaction effects in higher-order topological insulators. Our construction can also be applied to other lattice geometries, and extended to higher dimensions, where π -flux models can exhibit 4-fold ground-state degeneracy [54]; see also Refs. [66–71] on various π -flux models with frustration.

The chiral dynamics studied in our work can also be relevant to nonlinear photonic systems [72–77], e.g. arrays of coupled optical waveguides [78], upon injection of light with the appropriate relative phase pattern among the sites of an elementary plaquette [79]. This would provide an alternative framework to explore orbital physics [80–82] in the nonlinear regime.

Acknowledgements. The authors are pleased to acknowledge discussions with L. Barbiero, I. Carusotto, N. R. Cooper, J. Dalibard, E. Demler, O. K. Diessel, A. Eckardt, D. González-Cuadra, G. Juzeliūnas, L. Peralta Gavensky, T. Zache and Qi Zhou. This work is supported by the ERC Starting Grant TopoCold, the Fonds De La Recherche Scientifique (FRS-FNRS, Belgium), the QuantERA grant MAQS via the Austrian Science Fund FWF No I4391-N and the Rita Levi Montalcini Program through the fellowship DILLLEVI22.01.

* marco.diliberto@unipd.it

† nathan.goldman@ulb.be

- [1] K. W. Madison, F. Chevy, W. Wohlleben, and J. Dalibard, *Phys. Rev. Lett.* **84**, 806 (2000).
- [2] J. R. Abo-Shaer, C. Raman, J. M. Vogels, and W. Ketterle, *Science* **292**, 476 (2001).
- [3] N. Cooper, *Advances in Physics* **57**, 539 (2008).
- [4] S. M. Girvin, in *The Quantum Hall Effect* (Springer, 2005) pp. 133–162.
- [5] S. Tung, V. Schweikhard, and E. A. Cornell, *Phys. Rev. Lett.* **97**, 240402 (2006).
- [6] J. Struck, M. Weinberg, C. Ölschläger, P. Windpassinger, J. Simonet, K. Sengstock, R. Höppner, P. Hauke, A. Eckardt, M. Lewenstein, *et al.*, *Nature Physics* **9**, 738 (2013).
- [7] G. Jotzu, M. Messer, R. Desbuquois, M. Lebrat, T. Uehlinger, D. Greif, and T. Esslinger, *Nature* **515**, 237 (2014).
- [8] N. R. Cooper, J. Dalibard, and I. B. Spielman, *Rev. Mod. Phys.* **91**, 015005 (2019).
- [9] J. Dalibard, F. Gerbier, G. Juzeliūnas, and P. Öhberg, *Rev. Mod. Phys.* **83**, 1523 (2011).
- [10] N. Goldman, G. Juzeliūnas, P. Öhberg, and I. B. Spielman, *Reports on Progress in Physics* **77**, 126401 (2014).
- [11] D. Jaksch and P. Zoller, *New Journal of Physics* **5**, 56 (2003).
- [12] F. Gerbier and J. Dalibard, *New Journal of Physics* **12**, 033007 (2010).
- [13] N. R. Cooper, *Phys. Rev. Lett.* **106**, 175301 (2011).
- [14] A. Celi, P. Massignan, J. Ruseckas, N. Goldman, I. B. Spielman, G. Juzeliūnas, and M. Lewenstein, *Phys. Rev. Lett.* **112**, 043001 (2014).
- [15] V. Lienhard, P. Scholl, S. Weber, D. Barredo, S. de Léséleuc, R. Bai, N. Lang, M. Fleischhauer, H. P. Büchler, T. Lahaye, and A. Browaeys, *Phys. Rev. X* **10**, 021031 (2020).
- [16] M. Atala, M. Aidelsburger, M. Lohse, J. T. Barreiro, B. Paredes, and I. Bloch, *Nature Physics* **10**, 588 (2014).
- [17] B. Stuhl, H.-I. Lu, L. Ayccock, D. Genkina, and I. Spielman, *Science* **349**, 1514 (2015).
- [18] M. Mancini, G. Pagano, G. Cappellini, L. Livi, M. Rider, J. Catani, C. Sias, P. Zoller, M. Inguscio, M. Dalmonte, *et al.*, *Science* **349**, 1510 (2015).
- [19] F. A. An, E. J. Meier, and B. Gadway, *Science Advances* **3**, e1602685 (2017).
- [20] T. Chalopin, T. Satoor, A. Evrard, V. Makhlov, J. Dalibard, R. Lopes, and S. Nascimbene, *Nature Physics* **16**, 1017 (2020).
- [21] A. Isacsson and S. M. Girvin, *Phys. Rev. A* **72**, 053604 (2005).
- [22] W. V. Liu and C. Wu, *Phys. Rev. A* **74**, 013607 (2006).
- [23] X. Li and W. V. Liu, *Reports on Progress in Physics* **79**, 116401 (2016).
- [24] C. Wu, W. V. Liu, J. Moore, and S. D. Sarma, *Phys. Rev. Lett.* **97**, 190406 (2006).
- [25] C. Wu, *Phys. Rev. Lett.* **100**, 200406 (2008).
- [26] C. Wu, *Phys. Rev. Lett.* **101**, 186807 (2008).
- [27] E. Zhao and W. V. Liu, *Phys. Rev. Lett.* **100**, 160403 (2008).
- [28] K. Sun, W. V. Liu, A. Hemmerich, and S. Das Sarma, *Nature Physics* **8**, 67 (2012).
- [29] X. Li, Z. Zhang, and W. V. Liu, *Phys. Rev. Lett.* **108**, 175302 (2012).
- [30] F. Pinheiro, G. M. Bruun, J.-P. Martikainen, and J. Larson, *Phys. Rev. Lett.* **111**, 205302 (2013).
- [31] Y. Li, J. Yuan, X. Zhou, and X. Li, *Phys. Rev. Res.* **3**, 033274 (2021).
- [32] M. Di Liberto, A. Hemmerich, and C. Morais Smith, *Phys. Rev. Lett.* **117**, 163001 (2016).
- [33] Z.-F. Xu, L. You, A. Hemmerich, and W. V. Liu, *Phys. Rev. Lett.* **117**, 085301 (2016).
- [34] T. Müller, S. Fölling, A. Widera, and I. Bloch, *Phys. Rev. Lett.* **99**, 200405 (2007).
- [35] G. Wirth, M. Ölschläger, and A. Hemmerich, *Nature Physics* **7**, 147 (2011).
- [36] M. Ölschläger, G. Wirth, and A. Hemmerich, *Phys. Rev. Lett.* **106**, 015302 (2011).
- [37] X.-Q. Wang, G.-Q. Luo, J.-Y. Liu, W. V. Liu, A. Hemmerich, and Z.-F. Xu, *Nature* **596**, 227 (2021).
- [38] S. Jin, W. Zhang, X. Guo, X. Chen, X. Zhou, and X. Li, *Phys. Rev. Lett.* **126**, 035301 (2021).

- [39] P. Roushan, C. Neill, A. Megrant, Y. Chen, R. Babush, R. Barends, B. Campbell, Z. Chen, B. Chiaro, A. Dunsworth, A. Fowler, E. Jeffrey, J. Kelly, E. Lucero, J. Mutus, P. J. J. O'Malley, M. Neeley, C. Quintana, D. Sank, A. Vainsencher, J. Wenner, T. White, E. Kapit, H. Neven, and J. Martinis, *Nature Physics* **13**, 146 (2017).
- [40] J. Bibo, I. Lovas, Y. You, F. Grusdt, and F. Pollmann, *Phys. Rev. B* **102**, 041126 (2020).
- [41] M. Di Liberto, N. Goldman, and G. Palumbo, *Nature Communications* **11**, 5942 (2020).
- [42] "See supplemental material for more details."
- [43] S. D. Huber and E. Altman, *Phys. Rev. B* **82**, 184502 (2010).
- [44] G. Möller and N. R. Cooper, *Phys. Rev. Lett.* **108**, 045306 (2012).
- [45] Notice that the two symmetries (time-reversal and orbital \mathbb{Z}_2) are not equivalent. If the Hamiltonian had a term $\delta E \hat{d}_1^\dagger \hat{d}_1$, this would explicitly break the \mathbb{Z}_2 orbital symmetry while preserving time-reversal. However, for sufficiently small δE , the ground-state would still be a time-reversal broken state $(\sin \alpha \hat{d}_1^\dagger \pm i \cos \alpha \hat{d}_2^\dagger)^N |0\rangle$, where α can be expressed in terms of δE .
- [46] X. Li, A. Paramekanti, A. Hemmerich, and W. V. Liu, *Nature Communications* **5**, 3205 (2014).
- [47] J. Vargas, M. Nuske, R. Eichberger, C. Hippler, L. Mathey, and A. Hemmerich, *Phys. Rev. Lett.* **126**, 200402 (2021).
- [48] I. B. Spielman, *Annalen der Physik* **525**, 797 (2013).
- [49] N. Goldman, J. Dalibard, A. Dauphin, F. Gerbier, M. Lewenstein, P. Zoller, and I. B. Spielman, *Proceedings of the National Academy of Sciences* **110**, 6736 (2013).
- [50] X.-Y. Dong, A. G. Grushin, J. Motruk, and F. Pollmann, *Phys. Rev. Lett.* **121**, 086401 (2018).
- [51] P. Weinberg and M. Bukov, *SciPost Phys.* **7**, 20 (2019).
- [52] L.-H. Wu and X. Hu, *Phys. Rev. Lett.* **114**, 223901 (2015).
- [53] V. G. Sala, D. D. Solnyshkov, I. Carusotto, T. Jacqmin, A. Lemaître, H. Terças, A. Nalitov, M. Abbarchi, E. Galopin, I. Sagnes, J. Bloch, G. Malpuech, and A. Amo, *Phys. Rev. X* **5**, 011034 (2015).
- [54] W. A. Benalcazar, B. A. Bernevig, and T. L. Hughes, *Science* **357**, 61 (2017).
- [55] L.-K. Lim, C. Morais Smith, and A. Hemmerich, *Phys. Rev. Lett.* **100**, 130402 (2008).
- [56] M. Fishman, S. R. White, and E. M. Stoudenmire, *SciPost Phys. Codebases*, 4 (2022).
- [57] P. Zanardi and N. Paunković, *Phys. Rev. E* **74**, 031123 (2006).
- [58] J. Carrasquilla, S. R. Manmana, and M. Rigol, *Phys. Rev. A* **87**, 043606 (2013).
- [59] R. Samajdar, W. W. Ho, H. Pichler, M. D. Lukin, and S. Sachdev, *Proceedings of the National Academy of Sciences*, *Proceedings of the National Academy of Sciences* **118**, e2015785118 (2021).
- [60] F. Kolley, M. Piraud, I. P. McCulloch, U. Schollwöck, and F. Heidrich-Meisner, *New Journal of Physics* **17**, 092001 (2015).
- [61] S. Greschner, M. Piraud, F. Heidrich-Meisner, I. P. McCulloch, U. Schollwöck, and T. Vekua, *Phys. Rev. Lett.* **115**, 190402 (2015).
- [62] Y. You, T. Devakul, F. J. Burnell, and T. Neupert, *Phys. Rev. B* **98**, 235102 (2018).
- [63] O. Dubinkin and T. L. Hughes, *Phys. Rev. B* **99**, 235132 (2019).
- [64] K. Kudo, T. Yoshida, and Y. Hatsugai, *Phys. Rev. Lett.* **123**, 196402 (2019).
- [65] D. González-Cuadra, *Phys. Rev. B* **105**, L020403 (2022).
- [66] M. Polini, R. Fazio, A. H. MacDonald, and M. P. Tosi, *Phys. Rev. Lett.* **95**, 010401 (2005).
- [67] S. Mukherjee, M. Di Liberto, P. Öhberg, R. R. Thomson, and N. Goldman, *Phys. Rev. Lett.* **121**, 075502 (2018).
- [68] M. Di Liberto, S. Mukherjee, and N. Goldman, *Phys. Rev. A* **100**, 043829 (2019).
- [69] M. Kremer, I. Petrides, E. Meyer, M. Heinrich, O. Zilberberg, and A. Szameit, *Nature communications* **11**, 1 (2020).
- [70] J. Zurita, C. Creffield, and G. Platero, *Quantum* **5**, 591 (2021).
- [71] L. Barbiero, J. Cabedo, M. Lewenstein, L. Tarruell, and A. Celi, *arXiv:2212.06112* (2022).
- [72] M. C. Rechtsman, J. M. Zeuner, Y. Plotnik, Y. Lumer, D. Podolsky, F. Dreisow, S. Nolte, M. Segev, and A. Szameit, *Nature* **496**, 196 (2013).
- [73] M. Hafezi, S. Mittal, J. Fan, A. Migdall, and J. Taylor, *Nature Photonics* **7**, 1001 (2013).
- [74] T. Ozawa, H. M. Price, A. Amo, N. Goldman, M. Hafezi, L. Lu, M. C. Rechtsman, D. Schuster, J. Simon, O. Zilberberg, and I. Carusotto, *Rev. Mod. Phys.* **91**, 015006 (2019).
- [75] S. Mukherjee and M. C. Rechtsman, *Science* **368**, 856 (2020).
- [76] D. Smirnova, D. Leykam, Y. Chong, and Y. Kivshar, *Applied Physics Reviews* **7**, 021306 (2020).
- [77] A. Muñoz de las Heras and I. Carusotto, *Phys. Rev. A* **104**, 043501 (2021).
- [78] A. Szameit and S. Nolte, *Journal of Physics B: Atomic, Molecular and Optical Physics* **43**, 163001 (2010).
- [79] Nonlinearities in waveguides are attractive, $g < 0$, but we verified that chiral dynamics exists for both positive and negative U .
- [80] M. Milićević, T. Ozawa, G. Montambaux, I. Carusotto, E. Galopin, A. Lemaître, L. Le Gratiet, I. Sagnes, J. Bloch, and A. Amo, *Phys. Rev. Lett.* **118**, 107403 (2017).
- [81] C. E. Whittaker, E. Cancellieri, P. M. Walker, D. R. Gulevich, H. Schomerus, D. Vaitiekus, B. Royall, D. M. Whittaker, E. Clarke, I. V. Iorsh, I. A. Shelykh, M. S. Skolnick, and D. N. Krizhanovskii, *Phys. Rev. Lett.* **120**, 097401 (2018).
- [82] F. Scafirimuto, D. Urbonas, M. A. Becker, U. Scherf, R. F. Mahrt, and T. Stöferle, *Communications Physics* **4**, 39 (2021).

SUPPLEMENTAL MATERIAL

Effective theory. The single-particle Hamiltonian describing the π -flux plaquette,

$$\hat{H}_0 = -J \left(e^{i\pi} \hat{b}_1^\dagger \hat{b}_2 + \hat{b}_2^\dagger \hat{b}_4 + \hat{b}_4^\dagger \hat{b}_3 + \hat{b}_3^\dagger \hat{b}_1 + \text{H.c.} \right), \quad (\text{S1})$$

admits the eigenstates $|d_i\rangle = \sum_j \mathcal{U}_{ij}^{-1} |b_j\rangle$, with $i = 1, \dots, 4$ and

$$\mathcal{U} = \begin{pmatrix} \frac{1}{2} & -\frac{1}{2} & -\frac{1}{2} & \frac{1}{2} \\ 0 & \frac{1}{\sqrt{2}} & 0 & \frac{1}{\sqrt{2}} \\ \frac{1}{\sqrt{2}} & 0 & \frac{1}{\sqrt{2}} & 0 \\ \frac{1}{2} & \frac{1}{2} & -\frac{1}{2} & -\frac{1}{2} \end{pmatrix}. \quad (\text{S2})$$

The corresponding eigenvalues are $\epsilon_{1,2} = -\sqrt{2}J$ and $\epsilon_{3,4} = \sqrt{2}J$. The single-particle gap $\Delta\epsilon = 2\sqrt{2}J$, together with the weak coupling condition $g/J \ll 1$ considered in this work, allows us to project the full interacting Hamiltonian onto the lowest energy single-particle states and to neglect virtual processes involving the high energy modes. Specifically, this projection is achieved by decomposing the operators as $\hat{b}_i = \sum_{ij} \mathcal{U}_{ij} \hat{d}_j$ and by dropping the contributions from $\hat{d}_{3,4}$. We note that these terms would be relevant to construct an effective theory in second order perturbation theory (here, we limit ourselves to the lowest order contribution). The Hubbard interaction

$$\hat{H}_{\text{int}} = \frac{U}{2} \sum_i \hat{n}_i (\hat{n}_i - 1), \quad (\text{S3})$$

thus becomes

$$\begin{aligned} \hat{H}_{\text{int}}^{\text{eff}} \equiv \hat{P} \hat{H}_{\text{int}} \hat{P} &= \frac{3U}{16} \left(\hat{d}_1^\dagger \hat{d}_1^\dagger \hat{d}_1 \hat{d}_1 + \hat{d}_2^\dagger \hat{d}_2^\dagger \hat{d}_2 \hat{d}_2 \right) \\ &+ \frac{U}{4} \hat{d}_1^\dagger \hat{d}_2^\dagger \hat{d}_1 \hat{d}_2 + \frac{U}{16} \left(\hat{d}_1^\dagger \hat{d}_1^\dagger \hat{d}_2 \hat{d}_2 + \hat{d}_2^\dagger \hat{d}_2^\dagger \hat{d}_1 \hat{d}_1 \right), \end{aligned} \quad (\text{S4})$$

where \hat{P} is the projection operator. Note the orbital-changing terms in the second line of Eq. (S4). Let us define the density operator $\hat{n} = \hat{d}_1^\dagger \hat{d}_1 + \hat{d}_2^\dagger \hat{d}_2$ and the angular momentum operator $\hat{L}_z = i(\hat{d}_1^\dagger \hat{d}_2 - \hat{d}_2^\dagger \hat{d}_1)$. The interaction Hamiltonian finally reads

$$\hat{H}_{\text{int}}^{\text{eff}} = \frac{3U}{16} \hat{n}^2 - \frac{U}{16} \hat{L}_z^2 - \frac{U}{8} \hat{n}. \quad (\text{S5})$$

As $[\hat{n}, \hat{L}_z] = 0$, the eigenstates of $\hat{H}_{\text{int}}^{\text{eff}}$ can be written in terms of the eigenstates of \hat{L}_z , which we indicate as $|\pm\rangle \equiv \hat{d}_\pm^\dagger |0\rangle$, where $\hat{d}_\pm^\dagger = (\hat{d}_1^\dagger \pm i\hat{d}_2^\dagger)/\sqrt{2}$, and satisfying $\hat{L}_z |\pm\rangle = \pm |\pm\rangle$. A generic many-body eigenstate can therefore be written as

$$|n_+, n_-\rangle = \frac{1}{\sqrt{n_+! n_-!}} (\hat{d}_+^\dagger)^{n_+} (\hat{d}_-^\dagger)^{n_-} |0\rangle, \quad (\text{S6})$$

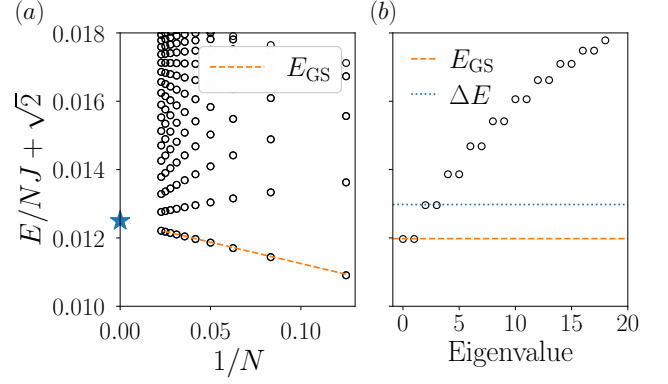


Figure S1. Spectrum of the effective model. (a) Energy spectrum obtained with exact diagonalization for $g = UN = 0.1J$ as a function of number of particles N . The dashed line is the analytical ground state energy E_{GS} (see text), whereas the star is the mean-field result for $N \rightarrow \infty$. (b) Spectrum for $N = 24$ bosons. The dashed and dotted lines indicate the analytical values of the ground state energy $E_{\text{GS}} = Ng/8 - g/8$ and of the lowest energy excitation $\Delta E = g/4 - U/4$.

with $N = n_+ + n_-$. The corresponding eigenvalues read

$$E(n_+, n_-) = \frac{3U}{16} N^2 - \frac{U}{16} (n_+ - n_-)^2 - \frac{U}{8} N. \quad (\text{S7})$$

As only one between n_- and n_+ is independent, there are in total $N + 1$ states. Inspection of this expression shows that there are two degenerate ground states corresponding to $n_+ = N$ or $n_- = N$ with interaction energy $E_{\text{GS}} = Ng/8 - g/8$. These results correspond to the mean-field results, detailed in the main text, for $N \rightarrow \infty$. As here we are solving for the exact eigenstates, we also have found a beyond-mean field correction to the energy that does not scale with the number of particles N . Let us consider the ground state with $n_+ = N$ and $n_- = 0$. In the particle-conserving framework, the lowest-energy excitation corresponds to a single-particle excitation of the form $n'_+ = n_+ - 1 = N - 1$ and $n'_- = n_- + 1 = 1$, namely a particle transferred to a state with opposite chirality. This corresponds to a change in the angular momentum, and the energy for this excitation is

$$\Delta E = \frac{g}{4} - \frac{U}{4} > 0. \quad (\text{S8})$$

This is exactly the result that we obtained within the Bogoliubov theory for the gapped mode. We therefore have identified that the gapped mode describes a single particle excitation corresponding to flipping the angular momentum of a particle in the condensate. The mean-field equations of motion can be derived from the Lagrangian (7), which read

$$\begin{aligned} i\partial_t d_1 &= \frac{3U}{8} (n_1 + n_2) d_1 - i\frac{U}{8} L_z d_2 - \frac{V(t)}{2} d_1, \\ i\partial_t d_2 &= \frac{3U}{8} (n_1 + n_2) d_2 + i\frac{U}{8} L_z d_1 + \frac{V(t)}{2} d_2, \end{aligned} \quad (\text{S9})$$

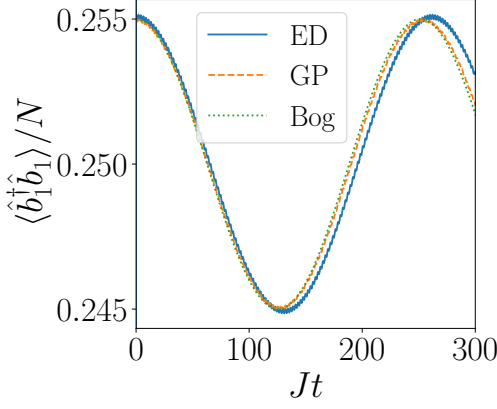


Figure S2. Comparison of the impurity dynamics obtained from exact diagonalization, Gross-Pitaevskii and Bogoliubov theory. Parameters as in the main text.

where we included also the drive $V(t)$. These equations were numerically solved in the presence of the drive to excite the collective mode via a time-periodic modulation.

Bogoliubov theory. Here we show how Bogoliubov theory can be used to describe the 4-sites GP dynamics for the excited mode. After replacing $\hat{d}_1 = \langle \hat{d}_1 \rangle + \delta \hat{d}_1$, $\hat{d}_2 = \langle \hat{d}_2 \rangle + \delta \hat{d}_2$ in \hat{H}_{eff} and analogous relations for

the Hermitian conjugates, we obtain the single-plaquette Bogoliubov Hamiltonian $\hat{H}_{\text{Bog}} = \omega_0 \hat{\beta}^\dagger \hat{\beta}$, where $\hat{\beta}^\dagger = (i \delta \hat{d}_1^\dagger + \delta \hat{d}_2^\dagger) / \sqrt{2}$. In terms of the sites fluctuation operators $\delta \hat{b}_i^{(\dagger)}$, the Bogoliubov Hamiltonian governing the dynamics of the excitations reads

$$\hat{H}_{\text{Bog}} = \sum_{i,j} \left(\tilde{J}_{ij} \delta \hat{b}_i^\dagger \delta \hat{b}_j + \text{H.c.} \right), \quad (\text{S10})$$

where the nearest-neighbor couplings are $\tilde{J}_{21} = -(\omega_0/4)e^{i\pi/4}$, $\tilde{J}_{13} = \tilde{J}_{34} = \tilde{J}_{42} = -\tilde{J}_{21}$ and the next-nearest-neighbor ones $\tilde{J}_{14} = \tilde{J}_{32} = (\omega_0/4)e^{i\pi/2}$. Notice the appearance of couplings between nearest- and next-nearest-neighbor sites that are proportional to ω_0 . We now evolve the mean-field initial impurity state, obtained by adding an onsite potential $-\Delta \hat{b}_1^\dagger \hat{b}_1$ as in the main text to find the ground state and then quenching $\Delta \rightarrow 0$, with such free Hamiltonian. The results of the dynamics under \hat{H}_{Bog} is shown in Fig. S2 and agrees with the GP and ED results.

Decay rate of the gapped mode. Under the mean-field substitution $\hat{d}_{1,\mathbf{r}} \rightarrow \sqrt{\rho/2} + \delta \hat{d}_{1,\mathbf{r}}$ and $\hat{d}_{2,\mathbf{r}} \rightarrow i\sqrt{\rho/2} + \delta \hat{d}_{2,\mathbf{r}}$, the BBH interacting model can be decomposed into $\hat{H} = \hat{H}^{(0)} + \hat{H}^{(2)} + \hat{H}^{(3)}$, where each term $\hat{H}^{(i)}$ is defined by having the corresponding powers of operators $\delta \hat{d}_{\sigma,\mathbf{r}}^{(\dagger)}$. The linear term vanishes by choosing the chemical potential accordingly. The quadratic (Bogoliubov approximation) term $\hat{H}^{(2)}$ reads

$$\begin{aligned} \hat{H}^{(2)} = & -\frac{J'}{2\sqrt{2}} \sum_{\mathbf{r},\nu} \left(\delta \hat{d}_{1,\mathbf{r}}^\dagger \delta \hat{d}_{1,\mathbf{r}+\mathbf{e}_\nu} + \text{H.c.} \right) - \frac{J'}{2\sqrt{2}} \sum_{\mathbf{r},\nu} \left(\delta \hat{d}_{2,\mathbf{r}}^\dagger \delta \hat{d}_{2,\mathbf{r}+\mathbf{e}_\nu} + \text{H.c.} \right) \\ & - \sqrt{2} J \sum_{\mathbf{r}} \left(\delta \hat{d}_{1,\mathbf{r}}^\dagger \delta \hat{d}_{1,\mathbf{r}} + \delta \hat{d}_{2,\mathbf{r}}^\dagger \delta \hat{d}_{2,\mathbf{r}} \right) - \mu \sum_{\mathbf{r}} \left(\delta \hat{d}_{1,\mathbf{r}}^\dagger \delta \hat{d}_{1,\mathbf{r}} + \delta \hat{d}_{2,\mathbf{r}}^\dagger \delta \hat{d}_{2,\mathbf{r}} \right) \\ & + \frac{g}{2} \sum_{\mathbf{r}} \left(\delta \hat{d}_{1,\mathbf{r}}^\dagger \delta \hat{d}_{1,\mathbf{r}} + \delta \hat{d}_{2,\mathbf{r}}^\dagger \delta \hat{d}_{2,\mathbf{r}} \right) + \frac{g}{16} \sum_{\mathbf{r}} \left(\delta \hat{d}_{1,\mathbf{r}}^\dagger \delta \hat{d}_{1,\mathbf{r}}^\dagger + \delta \hat{d}_{1,\mathbf{r}} \delta \hat{d}_{1,\mathbf{r}} \right) \\ & - \frac{g}{16} \sum_{\mathbf{r}} \left(\delta \hat{d}_{2,\mathbf{r}}^\dagger \delta \hat{d}_{2,\mathbf{r}}^\dagger + \delta \hat{d}_{2,\mathbf{r}} \delta \hat{d}_{2,\mathbf{r}} \right) + i \frac{g}{8} \sum_{\mathbf{r}} \left(\delta \hat{d}_{1,\mathbf{r}}^\dagger \delta \hat{d}_{2,\mathbf{r}}^\dagger - \delta \hat{d}_{1,\mathbf{r}} \delta \hat{d}_{2,\mathbf{r}} \right). \end{aligned} \quad (\text{S11})$$

that can be recast in momentum space after introducing the fluctuation field operator $\delta \hat{\Psi}_{\mathbf{k}} \equiv (\delta \hat{d}_{1,\mathbf{k}}, \delta \hat{d}_{2,\mathbf{k}}, \delta \hat{d}_{1,-\mathbf{k}}^\dagger, \delta \hat{d}_{2,-\mathbf{k}}^\dagger)^T$ in order to obtain the Bogoliubov Hamiltonian $\hat{H}^{(2)} = \frac{1}{2} \sum_{\mathbf{k}} \delta \hat{\Psi}_{\mathbf{k}}^\dagger H(\mathbf{k}) \delta \hat{\Psi}_{\mathbf{k}}$ where

$$H(\mathbf{k}) = \begin{pmatrix} \Sigma_{\mathbf{k}} & \Delta \\ \Delta^\dagger & \Sigma_{\mathbf{k}} \end{pmatrix}, \quad \text{with } \Delta = \frac{g}{8} \begin{pmatrix} 1 & i \\ i & -1 \end{pmatrix}, \quad (\text{S12})$$

and $\Sigma_{\mathbf{k}} = (\epsilon_{\mathbf{k}} - \mu + g/2) \mathcal{I}_{2 \times 2}$, $\epsilon_{\mathbf{k}} = -\sqrt{2}J - J'(\cos k_x a + \cos k_y a) / \sqrt{2}$ and $\mu = -\sqrt{2}(J + J') + g/4$. Diagonalization yields $\hat{H}^{(2)} = \sum_{\mathbf{k} \neq 0, \alpha} \omega_{\alpha,\mathbf{k}} \hat{\beta}_{\alpha,\mathbf{k}}^\dagger \hat{\beta}_{\alpha,\mathbf{k}}$, with $\alpha = 1, 2$, where $\hat{\beta}_{\alpha,\mathbf{k}}^\dagger$ creates a Bogoliubov quasiparticle and the spectrum reads $\omega_{1,\mathbf{k}} = \sqrt{\xi_{\mathbf{k}}(\xi_{\mathbf{k}} + g)}$ and $\omega_{2,\mathbf{k}} = g/4 + \xi_{\mathbf{k}}$ with $\xi_{\mathbf{k}} \equiv -J'(\cos k_x a + \cos k_y a - 2) / \sqrt{2}$.

For the decay of the gapped mode, we are interested in the cubic term, $\hat{H}^{(3)}$, that couple Bogoliubov quasiparticles of different branches thus determining the leading channel for the the decay of the excited mode. The cubic order

reads

$$\begin{aligned}
\frac{16}{U} \sqrt{\frac{2}{\rho}} \hat{H}^{(3)} &= +3 \delta \hat{d}_{1,r}^\dagger \delta \hat{d}_{1,r} \delta \hat{d}_{1,r} - 3i \delta \hat{d}_{1,r}^\dagger \delta \hat{d}_{1,r} \delta \hat{d}_{2,r} - i \delta \hat{d}_{1,r}^\dagger \delta \hat{d}_{2,r} \delta \hat{d}_{1,r} + \delta \hat{d}_{1,r}^\dagger \delta \hat{d}_{2,r} \delta \hat{d}_{2,r} \\
&\quad - i \delta \hat{d}_{2,r}^\dagger \delta \hat{d}_{1,r} \delta \hat{d}_{1,r} - \delta \hat{d}_{2,r}^\dagger \delta \hat{d}_{1,r} \delta \hat{d}_{2,r} + 3 \delta \hat{d}_{2,r}^\dagger \delta \hat{d}_{2,r} \delta \hat{d}_{1,r} - 3i \delta \hat{d}_{2,r}^\dagger \delta \hat{d}_{2,r} \delta \hat{d}_{2,r} \\
&\quad + 3 \delta \hat{d}_{1,r} \delta \hat{d}_{1,r}^\dagger \delta \hat{d}_{1,r} + i \delta \hat{d}_{1,r} \delta \hat{d}_{1,r}^\dagger \delta \hat{d}_{2,r} - i \delta \hat{d}_{1,r} \delta \hat{d}_{2,r}^\dagger \delta \hat{d}_{1,r} + 3 \delta \hat{d}_{1,r} \delta \hat{d}_{2,r}^\dagger \delta \hat{d}_{2,r} \\
&\quad - 3i \delta \hat{d}_{2,r} \delta \hat{d}_{1,r}^\dagger \delta \hat{d}_{1,r} + \delta \hat{d}_{2,r} \delta \hat{d}_{1,r}^\dagger \delta \hat{d}_{2,r} - \delta \hat{d}_{2,r} \delta \hat{d}_{2,r}^\dagger \delta \hat{d}_{1,r} - 3i \delta \hat{d}_{2,r} \delta \hat{d}_{2,r}^\dagger \delta \hat{d}_{2,r} + \text{H.c.} \\
&= \sum_{ijk} A_{ijk} \delta \hat{d}_{i,r}^\dagger \delta \hat{d}_{j,r} \delta \hat{d}_{k,r} + B_{ijk} \delta \hat{d}_{i,r} \delta \hat{d}_{j,r}^\dagger \delta \hat{d}_{k,r} + C_{ijk} \delta \hat{d}_{i,r} \delta \hat{d}_{j,r}^\dagger \delta \hat{d}_{k,r} + D_{ijk} \delta \hat{d}_{i,r}^\dagger \delta \hat{d}_{j,r} \delta \hat{d}_{k,r}^\dagger,
\end{aligned}$$

where $C_{ijk} = A_{kji}^*$ and $D_{ijk} = B_{kji}^*$.

Let us denote the Bogoliubov transformation $\delta \hat{d}_{i,\mathbf{k}} = u_{ij,\mathbf{k}} \hat{\beta}_{j,\mathbf{k}} + v_{ij,\mathbf{k}}^* \hat{\beta}_{j,-\mathbf{k}}^\dagger$, we therefore find

$$\frac{16}{U} \sqrt{\frac{2}{\rho}} \hat{H}^{(3)} = \frac{1}{N_s^{1/2}} \sum_{\mathbf{q}} \hat{\beta}_{2,0} \hat{\beta}_{1,\mathbf{q}}^\dagger \hat{\beta}_{1,-\mathbf{q}} F_{\mathbf{q}} + \dots \quad (\text{S13})$$

where N_s is the number of sites and we retained only the terms determining the decay $|\beta_{2,0}\rangle \rightarrow |\beta_{1,\mathbf{q}}\beta_{1,-\mathbf{q}}\rangle$ and defined $F_{\mathbf{q}} = A_{ijk} P_{ijk,\mathbf{q}} + B_{ijk} Q_{ijk,\mathbf{q}} + C_{ijk} R_{ijk,\mathbf{q}} + D_{ijk} S_{ijk,\mathbf{q}}$, where

$$\begin{aligned}
P_{ijk,\mathbf{q}} &= u_{i1,\mathbf{q}}^* u_{j2,0} v_{k1,\mathbf{q}}^* + u_{i1,\mathbf{q}}^* v_{j1,-\mathbf{q}}^* u_{k2,0} \\
Q_{ijk,\mathbf{q}} &= u_{i2,0} u_{j1,\mathbf{q}}^* v_{k1,\mathbf{q}}^* + v_{i1,\mathbf{q}}^* u_{j1,\mathbf{q}}^* u_{k2,0} \\
R_{ijk,\mathbf{q}} &= u_{i1,\mathbf{q}}^* u_{j1,-\mathbf{q}}^* u_{k2,0} \\
S_{ijk,\mathbf{q}} &= u_{i1,\mathbf{q}}^* u_{j2,0} u_{k1,-\mathbf{q}}^*. \quad (\text{S14})
\end{aligned}$$

For $g \ll J'$, when the gap is much smaller than the bandwidth, we are in the small wavelength limit and the Bogoliubov Hamiltonian has the form

$$H_{\bar{\mathbf{q}}}^{(2)} = \begin{pmatrix} \tilde{q}^2 + \omega_0 & 0 & \omega_0/2 & i\omega_0/2 \\ 0 & \tilde{q}^2 + \omega_0 & i\omega_0/2 & -\omega_0/2 \\ \omega_0/2 & -i\omega_0/2 & \tilde{q}^2 + \omega_0 & 0 \\ -i\omega_0/2 & -\omega_0/2 & 0 & \tilde{q}^2 + \omega_0 \end{pmatrix}, \quad (\text{S15})$$

where we defined $\tilde{q}^2 = q^2(J'/2\sqrt{2})$ and $q^2 = q_x^2 + q_y^2$. The spectrum of $\Sigma_z H_{\bar{\mathbf{q}}}^{(2)}$ reads $\epsilon_{1,\bar{\mathbf{q}}} = \sqrt{\tilde{q}^2(\tilde{q}^2 + 2\omega_0)}$ and $\epsilon_{2,\bar{\mathbf{q}}} = \omega_0 + \tilde{q}^2$, whereas the Bogoliubov modes are

$$u_{ij,\bar{\mathbf{q}}} = \begin{pmatrix} -iu_{\bar{\mathbf{q}}} & \frac{i}{\sqrt{2}} \\ u_{\bar{\mathbf{q}}} & \frac{1}{\sqrt{2}} \end{pmatrix}, \quad v_{ij,\bar{\mathbf{q}}} = \begin{pmatrix} iv_{\bar{\mathbf{q}}} & 0 \\ v_{\bar{\mathbf{q}}} & 0 \end{pmatrix}, \quad (\text{S16})$$

with $u_{\bar{\mathbf{q}}}^2 = \frac{\xi_{\bar{\mathbf{q}}}^2}{2(\xi_{\bar{\mathbf{q}}}^2 - 1)}$ and $v_{\bar{\mathbf{q}}}^2 = \frac{1}{2(\xi_{\bar{\mathbf{q}}}^2 - 1)}$, and we defined $\xi_{\bar{\mathbf{q}}} = (\epsilon_{1,\bar{\mathbf{q}}} + \epsilon_{2,\bar{\mathbf{q}}})/\omega_0$. By direct calculation, we find that the only nonvanishing contribution to $F_{\mathbf{q}}$ is $F_{\mathbf{q}} = \sum_{ijk} C_{ijk} R_{ijk,\mathbf{q}} = -i\sqrt{2}u_{\bar{\mathbf{q}}}^2$.

The decay rate of the gapped mode can now be calculated by [S1]

$$\Gamma = \pi \sum_{\mathbf{q}} \delta(\omega_0 - 2\epsilon_{1,\mathbf{q}}) |\langle \beta_{1,\mathbf{q}} \beta_{1,-\mathbf{q}} | \hat{H}^{(3)} | \beta_{2,0} \rangle|^2, \quad (\text{S17})$$

and the resonance condition is satisfied when $\tilde{q}^2 = (\sqrt{2} - 1)\omega_0$ yielding $\xi_{\bar{\mathbf{q}}} = 1 + \sqrt{2}$. After transforming $N_s^{-1/2} \sum_{\mathbf{q}} \rightarrow 2\pi \int dq q$, we obtain

$$\begin{aligned}
\Gamma &= \frac{\sqrt{2}\pi^2 g U}{128 J'} \int d\tilde{q} \tilde{q} |F_{\tilde{q}}|^2 \delta(\omega - 2\epsilon_{1,\tilde{q}}) \\
&\approx \frac{0.73\pi^2 g U}{512 J'}. \quad (\text{S18})
\end{aligned}$$

Details on DMRG simulations. We have used the ITensor library to perform the DMRG calculations. All the simulations have been obtained by setting the truncation error threshold to 10^{-10} . The bond dimension threshold has been taken up to $\chi = 2000$ for some simulations that required a more accurate convergence and we have used up to 60 sweeps for the ground state search. In order to select a specific time-reversal broken ground state from the degenerate manifold, we have added a small uniform flux via a complex tunneling phase.

The fidelity susceptibility

$$\chi_{\mathcal{F}} = -(2/L_x) \lim_{\delta U \rightarrow 0} \partial^2 \mathcal{F} / \partial \delta U^2,$$

shown in Fig. 4(c) of the main text has been computed with a parabolic fit in δU of the fidelity $\mathcal{F}(\delta U) \equiv |\langle \Psi(U) | \Psi(U + \delta U) \rangle|$ for 10 values of $\delta U < 10^{-3} J$.

The charge gap shown in Fig. 4(d) $\Delta E_c = E(N+1) + E(N-1) - 2E(N)$, where N is the number of bosons, has been extrapolated from a linear fit in $1/L_x$, for $L_x = 32, 36, 40, 44, 48$.

Furthermore, we have checked that across the Mott transition, the spectrum remains doubly degenerate by computing the energy of few low-lying states.

[S1] L. Pitaevskii and S. Stringari, *Bose-Einstein Condensation and Superfluidity*, Oxford University Press (2016)